Cavitation erosion of silver plated coating considering thermodynamic effect

Shuji Hattori
Graduate School of Engineering,
University of Fukui, Japan

Keisuke Taruya
Student, Graduate School of Engineering,
University of Fukui, Japan

Kengo Kikuta
IHI Corporation, Japan

Hiroshi Tomaru
IHI Corporation, Japan

SUMMARY

Cavitation often occurs in inducer pumps of space rockets. Silver plated coatings on the inducer liner face the damage of cavitation. In this study, we carried out cavitation erosion tests using silver plated coatings with different thermodynamic parameters at a constant cavitation number. Then we carried out cavitation erosion tests using some liquids with the same thermodynamic parameter and cavitation number as liquid oxygen. The thermodynamic parameter Σ proposed by Brennen was used. The liquids used for the cavitation erosion tests were water, ethanol and hexane. We discuss the relation between the thermodynamic parameter and the mass loss rate, and the relation between acoustic impedance and the mass loss rate.

1. INTRODUCTION

Cavitation bubble collapse impact loads act repeatedly on a material surface to produce plastic deformation, crack initiation, crack growth and material removal. Cavitation erosion is a kind of fatigue phenomena. This phenomenon sometimes occurs on the components which contact flowing liquids such as pumps, piping systems and ship propellers. The erosion reduces the machine performance and the lifetime.

It is well known that cavitation occurs in inducer pumps used for space rockets [1-3]. Kamijo et al. [1] reported that backflow cavitation at the inlet of the pumps was suppressed by using a specially developed inducer with a different flow coefficient and a lower operating pressure. Yamada et al. [2] reported several examples of the accidents and unstable vibrations caused by cavitation in pumps. Uchiumi et al. [3] proposed an analytical method for cavity type evaluation in terms of the blade shape of the rocket inducer. Cavitation in the inducer may cause the erosion of the inducer and the liner. However, there have been no reports on cavitation erosion prevention methods or on the cavitation erosion behavior. Silver plated coatings are nowadays used for the clearance between pump inducers and liners to reduce the damage and the temperature rise when the inducer impeller contacts the coating [4, 5].

Hattori et al. [6] carried out cavitation erosion tests for silver plated coatings using a vibratory specimen method in deionized water, ethanol and liquid nitrogen. They discussed the effect of the test liquid and the temperature on the erosion mechanism. They found that cavitation erosion occurs in deionized water and ethanol, but it hardly occurs in liquid nitrogen. The reason was that bubbles generated by the pressure drop in liquid nitrogen did not collapse because the surrounding pressure increased to the atmospheric pressure, when the saturation pressure increased with the temperature rise. However, an experimental verification was not performed.

On the other hand, Brennen [7] found a thermodynamic parameter Σ based on the thermodynamics of single vapor bubbles in a flow system. He discussed the relation between the liquid temperature and the parameter Σ in hydrogen, oxygen, nitrogen, water, methane and freon. Brennen [8] also reported that the cavitation number of a pump head decreasing point in a centrifugal pump and a rocket inducer can be estimated by a nondimensional parameter Σ*. Recently, Watanabe et al. [9] reported a review of the thermodynamic effect of cavitation and a theoretical analysis. These researches discussed the thermodynamic effect on cavitation inception but not cavitation erosion.

In this study, we carried out cavitation erosion tests using silver plated coatings in liquids with different thermodynamic parameters at a constant cavitation number. Hardness tests were also carried out by using a Shore hardness tester as a function of the specimen temperature. Another set of cavitation erosion tests was carried out using three kinds of liquids with the same thermodynamic parameter and cavitation number as liquid oxygen condition. The fluids were water, ethanol and hexane. We discuss the relation between the thermodynamic parameter and the mass loss rate, and the relation between the acoustic impedance and the mass loss rate.

Proceedings of the Eighth International Symposium on Cavitation (CAV 2012)
Edited by Claus-Dieter OHL, Evert KLASEBOER, Siew Wan OHL, Shi Wei GONG and Boo Cheong KHOO.

ISBN: 978-981-07-2826-7 :: doi:10.3850/978-981-07-2826-7_103

2. EXPERIMENTAL SET UP

The specimen was a silver plated coating on a SUS304 base metal. Fig.1 shows the dimensions of a vibrating tip specimen with a diameter of 16mm. The coating was 150μm to 200μm in thickness and 10.5 mg/mm^3 in density. Table 1 shows the designation, coating metal, base metal, heat treatment, Vickers hardness and surface finish. The specimen was not heat-treated and the Vickers hardness (HV0.2) was 72.5. The surface finish was the same as the real inducer pump.

Cavitation erosion tests were carried out by using a vibratory apparatus as specified in the ASTM standard G32. The tests were carried out under controlled liquid temperature and pressure in a test chamber which was able to apply a pressure up to 0.7 MPa absolute and a temperature up to 423K. Figs.2(a) and (b) show a schematic drawing and a photograph of the test apparatus. The test temperature was controlled by a mantle heater and a temperature controller. Even when the mantle heater shut down at a predetermined temperature, the temperature continued to increase by cavitation bubble collapse. Therefore, we used a cooling coil in which water flowed to maintain the liquid temperature. The accuracy of the temperature control was ±2°C. Test pressure was controlled by pumping air in the sealed chamber using a compressor. The erosion tests began after attaching a specimen tip to the horn. Then, the pressure was applied and the test liquid was heated up to the predetermined temperature. The peak-to-peak displacement amplitude of the tip was 50μm. A precision balance (sensitivity 0.01mg) was used to measure the mass of the specimen, and the results were evaluated in terms of mass loss. A profilometer (KEYENCE LT-8010) was used to measure the profile of the eroded surface. A Shore hardness tester and a silicon rubber heater were used to measure the hardness as a function of the specimen temperature.

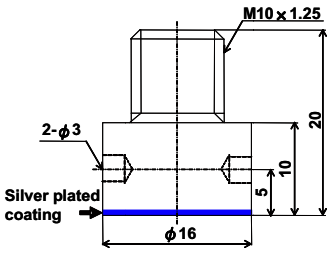

Fig.1 Dimension of specimen

3. RESULTS AND DISCUSSIONS

3.1 Cavitation erosion tests based on deionized water at 298K and 0.1MPa

Cavitation erosion tests were carried out using test liquids at several temperatures to evaluate the effect of the thermodynamic parameter on the cavitation erosion rate. The Σ proposed by Brennen [7] was used as the thermodynamic parameter. Σ depends on the liquid temperature and was defined by

$$\Sigma\,(T_\infty) = (\rho_v L) / (\rho_l c_{pl} T_\infty \alpha^{1/2}) \ , \qquad (1)$$

where T_∞ is the test temperature, ρ_v is the vapor density, ρ_l is the liquid density, L is the evaporative latent heat, c_{pl} is the constant pressure specific heat of the liquid and α_l is the thermal diffusivity of the liquid.

Fig.3 shows the variation in thermodynamic parameter Σ as a function of the nondimensional temperature calculated from the triple point to the critical point of the test liquid obtained from the p-T diagram (p:pressure and T:temperature). Each data point was calculated by Eq.(1). Σ increased with the temperature in all test liquids. Deionized water, ethanol and hexane were used in this study because of their easy handling.

Table 2 shows types of test liquid, test temperatures and thermodynamic parameter Σ. The test temperatures were determined based on deionized water at 298K (25°C, Σ = 7) and liquid oxygen at 90K (Σ=14500). In deionized water, cavitation erosion tests were carried out at temperatures of 298K(Σ=7), 324K(Σ=100), 352K(Σ=1028) and 401K(Σ=14500) so that Σ had similar intervals in the logarithmic scale.

Table 1 Condition of silver plated coating

Designation	Coating metal	Base metal	Heat treatment	HV0.2	Surface finish
C1	Ag	SUS304	None	72.5	Same as the real inducer pump

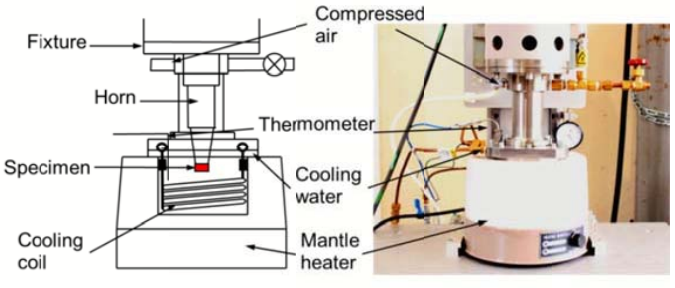

(a) Schematic drawing (b) Set up photograph

Fig.2 Test apparatus

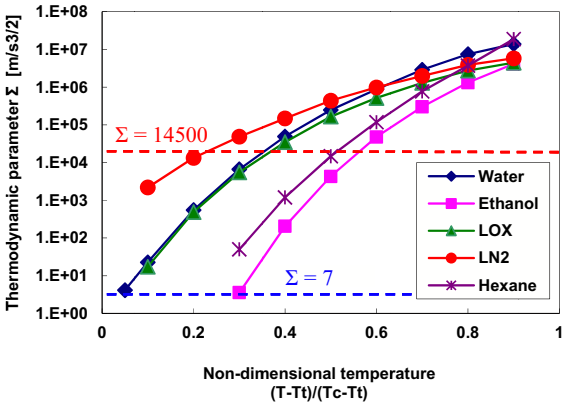

Fig.3 Thermodynamic parameter Σ

Table 2 Test conditions based on deionized water at 298K

Test liquid	Temperature [K]	Thermodynamic parameter Σ	Test pressure [MPa]	Saturated vapor pressure [MPa]	Liquid density [kg/m^3]	Cavitation number
Liquid oxygen	90	14500	–	0.0994	1142	–
Deionized water	298	7	0.101	0.0031	997	51.8
Deionized water	324	100	0.110	0.0129	988	51.8
Deionized water	352	1028	0.141	0.0452	972	51.8
Deionized water	401	14500	0.345	0.2530	937	51.8
Ethanol	303	225	0.101	0.0105	781	61.2
Ethanol	327	1950	0.110	0.0356	760	51.8
Ethanol	354	14500	0.184	0.1120	732	51.8
Ethanol	243	(0.9)	0.101	0.0002	831	63.9

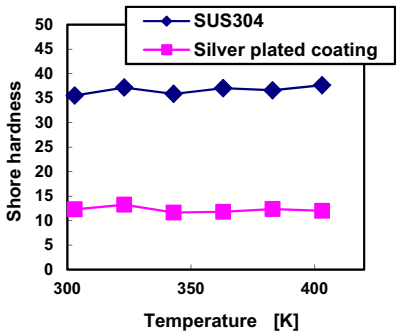

Fig.4 Relation between Shore hardness and temperature

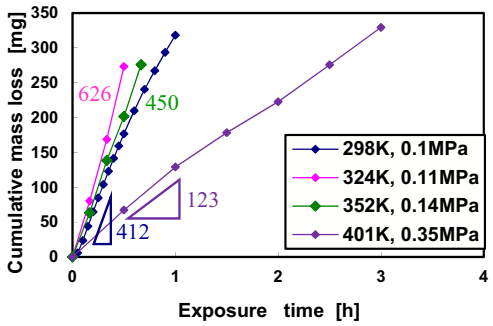

Fig. 5 Mass loss curves of deionized water

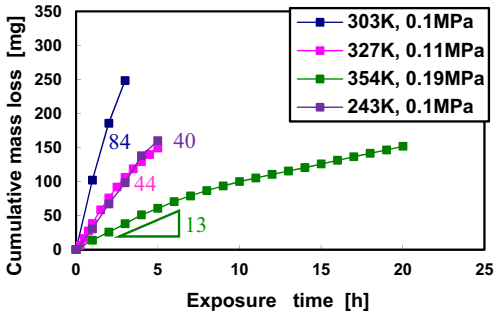

Fig. 6 Mass loss curves of ethanol

In ethanol, cavitation erosion tests were carried out at temperatures of 303K (Σ=225), 327K (Σ=1950) and 354K (Σ=14500). Table 2 also shows the test pressure (absolute), the saturated vapor pressure, the density of the liquid and the cavitation number. The test pressures were determined based on the cavitation number in deionized water at 298K and 0.1MPa. The cavitation number was defined as

$$\sigma = (p\text{-}p_v) / (1/2\rho_l v^2) \ , \qquad (2)$$

where p is the test pressure, p_v is the saturated vapor pressure and v is the flow velocity. It was difficult to measure the flow velocity in the vibratory specimen method. Therefore, we calculated the flow velocity from the oscillation frequency and the peak-to-peak displacement amplitude of the tip ($v = 50\times10^{-6}$m$\times2\times19500 = 1.95$m/s). If the flow velocity is assumed to be the same under all test conditions, the test pressure was given by

$$p_{ex} = (\rho_{l\_ex} / \rho_l) / (p - p_v) + p_{v\_ex} \ . \qquad (3)$$

The symbols with index *ex* indicate the test condition. The symbols without the index *ex* indicate the standard test condition. In ethanol, cavitation erosion tests at 303K and 243K were carried out at 0.1MPa, so that the cavitation numbers were different from σ = 51.8.

Before the cavitation erosion tests, Shore hardness tests were carried out for different specimen temperatures to examine whether the material hardness changes with the test temperature. The tests were carried out at several temperatures from 303K to 403K. The silver plated coating and the SUS304 base material were used in the hardness tests. Fig.4 shows the Shore hardness as a function of the test temperature. The Shore hardness of SUS304 at 303K is 35.5, and this value corresponds to a Vickers hardness of 236HV. This is a reasonable value for SUS304. The Shore hardness of SUS304 is almost constant irrespective of the test temperature. The Shore hardness of the silver plated coating at 303K is 12.3, and this value corresponds to a Vickers hardness of 73HV. This is also a reasonable value for the silver plated coating. The Shore hardness of silver plated coating is also nearly constant. Therefore, the temperature dependence of the material properties on cavitation erosion does not need to be considered, and only the temperature dependence of the liquid properties should be taken into account.

Fig.5 shows the cumulative mass loss curves at four different temperatures in deionized water. The incubation period does not appear clearly and the maximum rate stage

appears immediately at the beginning of each test for every temperature. The incubation period is extremely short because of the softness of the silver plated coating. The cumulative mass loss at 298K increases linearly in the early stage, and the mass loss rate decreases slightly after 40 minutes. The cumulative mass loss reaches 320mg after 1 hour. The curves at 324K and 352K are similar to that at 298K. The mass loss rate at 324K is the highest and reaches 280mg after 30minutes. The mass loss rate at 352K is higher than that at 298K and reaches 280mg after 40minutes. The mass loss rate at 401K is significantly lower than that in the other tests. The mass loss at 401K increases linearly and mass loss rate is about one third of that at 298K. The numerical value in Fig.6 shows the mass loss rate in the maximum rate stage.

Fig.6 shows cumulative mass loss curves at four temperatures in ethanol. The incubation period does not appear clearly and the maximum rate stage appears immediately at the beginning of each test at all temperatures similar to the tests in deionized water. The mass loss rates in ethanol are lower than that in deionized water. The tests took about six times longer than those in deionized water. The mass loss at 303K increases and the mass loss rate decreases gradually. The cumulative mass loss reaches 250mg after 3hours. The mass loss rate at 327K is lower than that at 303K. The mass loss at 327K increases and the mass loss rate decreases slightly similar to the curve at 303K. The cumulative mass loss reaches 160mg after 5hours. The mass loss rate at 354K is lower than that at 327K. The mass loss at 354K increases linearly and the mass loss rate decreases slightly after 5hours. The cumulative mass loss reached 130mg after 20 hours. The curve at 243K is similar to that at 327K and the cumulative mass loss reaches 160mg after 5 hours.

Fig.7 shows the mass loss rate in the maximum rate stage as a function of the thermodynamic parameter Σ. Brennen [7] found that the cavitation number at the drop point of pump head is constant up to a thermodynamic parameter Σ^* of 20 and that the cavitation number decreases for larger values of Σ^* [8]. Gross et al. [10] reported that the thermodynamic effect appeared at a Σ around 1.5 to 7.0×10^4 m/s$^{3/2}$ in liquid oxygen. Yoshida et al. reported that the thermodynamic effect appeared at a Σ of 4.7×10^4 m/s$^{3/2}$ [11] and for Σ around 1.3 to 8.1×10^4 m/s$^{3/2}$ [12] in liquid nitrogen. Kikuta et al. [13] reported that the thermodynamic effect appeared at Σ values of 3.8×10^4 m/s$^{3/2}$ and 1.3×10^4 m/s$^{3/2}$ in liquid nitrogen. Franc et al. [14] reported that the thermodynamic effect appeared at a Σ of 2.4 to 7.1×10^4

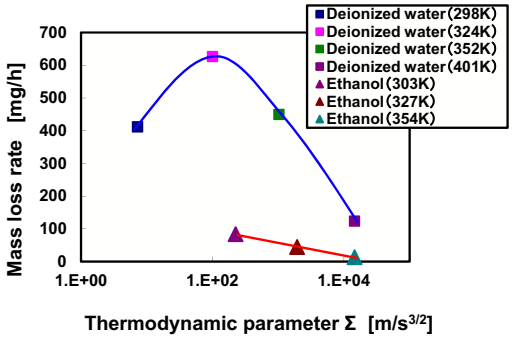

Fig. 7 Relation between mass loss and thermodynamic parameter Σ

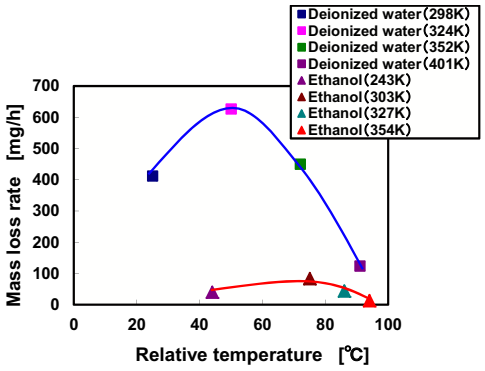

Fig. 8 Relation between mass loss and relative temperature

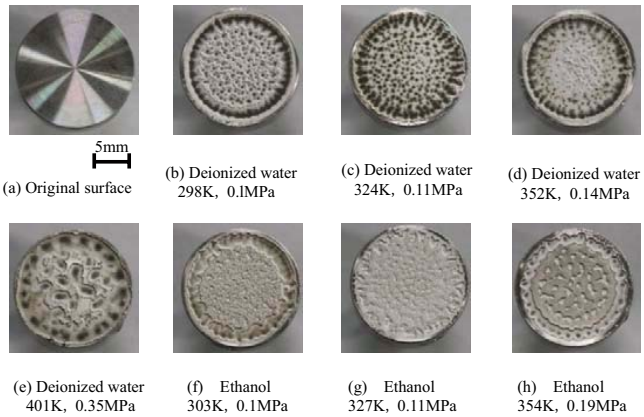

Fig.9 Eroded surfaces of test specimens

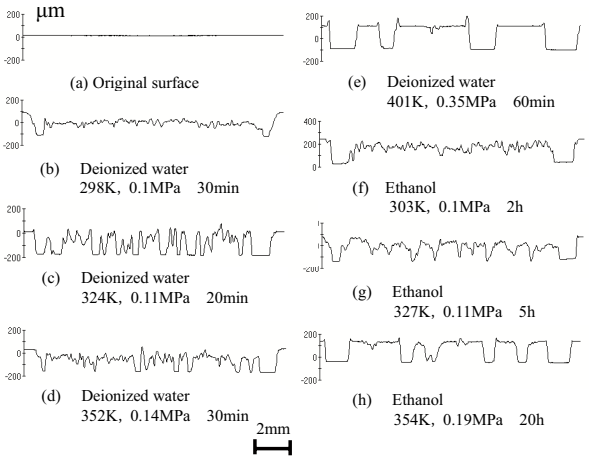

Fig.10 Surface profiles in deionized water and ethanol

$m/s^{3/2}$ in R114. In this study, thermodynamic effect appeared at a Σ of 100 $m/s^{3/2}$ or more showing a decrease in the mass loss. However, there are some differences in the mass loss rate depending on the test liquid. The result in this study is also different from Brennen's result [7] on the relation between the cavitation number at the drop point and Σ^*. Therefore, the mass loss rate was analyzed depending on the relative temperature. The relative temperature was defined by

Relative temperature =
(test temperature –melting point)/(boiling point –melting point) (4)

Fig.8 shows the mass loss rate as a function of the relative temperature. The curves are similar to our previous result [15]. We consider that the bubble number decreased with decreasing vapor pressure when the relative temperature was lowered to 25°C.

Fig.9 shows an original surface and surfaces after erosion tests. The original surface is very smooth. The specimen surface after each test was eroded deeply. In deionized water, the specimen surface was eroded deeper than that in ethanol.

Fig.10 shows examples of surface profiles obtained in deionized water and ethanol. The mass loss was about 150mg for all surface profiles in order to be able to compare the difference in the specimen surfaces at the same mass loss. The original surface was very smooth. In deionized water at 298K, the erosion proceeds severely in the peripheral area and uniformly in the middle area. At 324K, the specimen surface is divided into eroded and uneroded areas when compared to the surface at 298K. The surface at 352K was similar to that at 324K. At 401K, the specimen surface is clearly divided into eroded and uneroded areas. The eroded areas reach the base metal and the uneroded areas keep the original surface. In ethanol at 303K, it is observed that a ring area with 1 to 3mm width from the outer circumference is eroded deeply and a pear-skin surface appears inside the area. The surface profile at 327K was similar to that at 303K. At 354K, the surface was clearly divided into deep and shallow areas of erosion. The erosion depth in the deep erosion areas was about 200μm. However, the erosion depth in the shallow erosion areas was less than 30μm.

In conclusion, the thermodynamic effect appeared at a Σ of 100 $m/s^{3/2}$ or more and the mass loss rate decreased. When Σ decreased below 100$m/s^{3/2}$, the mass loss rate decreased with the decreasing bubble number due to the decrease in the saturated vapor pressure.

3.2 Cavitation erosion tests based on liquid nitrogen at 90K and 0.3MPa

The test conditions were determined based on liquid nitrogen at 90K and 0.3MPa. Table 3 shows the test liquid, temperature, thermodynamic parameter Σ, test pressure (absolute), saturated vapor pressure, density of the liquid and the cavitation number. The fluids used for the cavitation erosion tests were water, ethanol and hexane. The cavitation number is 92.4. The thermodynamic parameter Σ is 14500. The tests were carried out at the same thermodynamic parameter Σ and cavitation number as liquid oxygen at 90K and 0.3MPa. Therefore, the mass loss rate changes only with the acoustic impedance. Table 4 shows the acoustic impedance of test liquids.

Table 3 Test conditions based on LOX at 90K

Test liquid	Temperature [K]	Thermodynamic parameter Σ	Test pressure [MPa]	Saturated vapor pressure [MPa]	Cavitation number
Liquid oxygen	90	14500	0.300	0.0994	92.4
Deionized water	401	14500	0.418	0.2530	92.4
Ethanol	354	14500	0.241	0.1120	92.4
Hexane	343	14500	0.213	0.1050	92.4

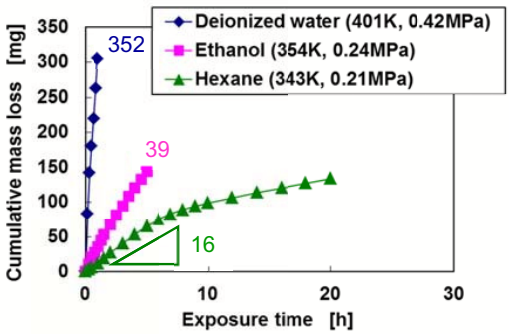

Fig. 11 Mass loss curves of deionized water, ethanol and hexane

Table 4 Acoustic impedance of test liquid

Test liquid	Density of liquid [kg/m^3]	Sound velocity [m/s]	Acoustic impedance [$kg/(m^2 s)$]
Liquid oxygen	1142	906	1.03×10^6
Deionized water	937	1508	1.41×10^6
Ethanol	732	1000	0.73×10^6
Hexane	612	868	0.53×10^6

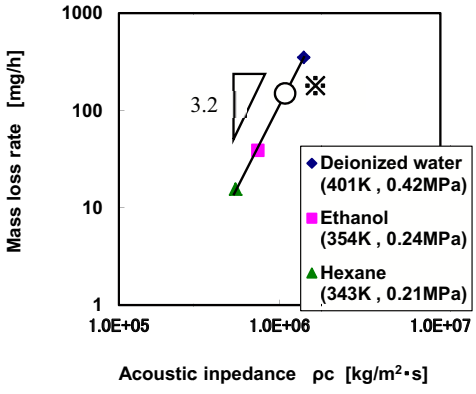

Fig. 12 Relation between mass loss rate and acoustic impedance

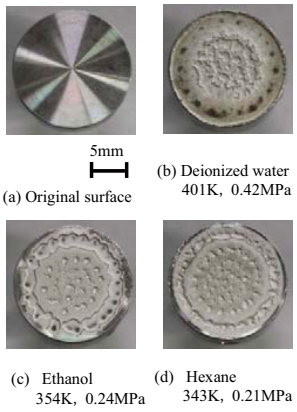

Fig. 13 Eroded surface of test specimens

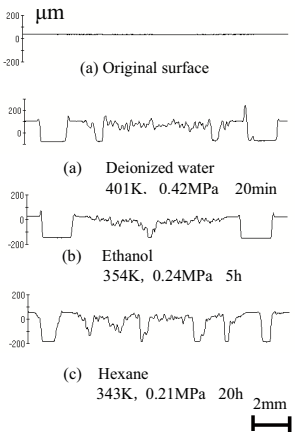

Fig. 14 Surface profiles

Fig.11 shows the cumulative mass loss curves. The incubation period does not appear clearly, and the maximum rate stage appears immediately after the beginning of each test for all test conditions. In deionized water, the mass loss reaches 80mg after 10 minutes. The mass loss increases by about 50mg every 10 minutes, and the cumulative mass loss reaches 310mg after 1 hour. In ethanol, the mass loss rate is lower than that in deionized water. The mass loss increases linearly in the initial stage, but the mass loss rate decreases gradually. The cumulative mass loss reaches 150mg after 5 hours. In hexane, the mass loss rate is lower than that in ethanol. The mass loss increases linearly and the mass loss rate decreases slightly after 5hours. The cumulative mass loss reaches 150mg after 20 hours. The values in figure show the mass loss rate of the maximum rate stage. The results show that mass loss rate increases with the acoustic impedance.

Fig.12 shows the mass loss rate as a function of the acoustic impedance. The mass loss rate as a function of acoustic impedance increases linearly on a log-log scale. A straight line is obtained with a slope of 3.2. This slope is similar to that in Wilson's study [16]. This means that the mass loss rate can be evaluated in terms of the acoustic impedance if the other conditions are kept constant. Furthermore, the mass loss rate in liquid oxygen was shown as a circle in Fig.12. The mass loss rate can be estimated according to this line.

Fig.13 shows an original surface and surfaces after the tests. The original surface is smooth. After the tests, specimen surfaces are eroded deeply. The shape of surfaces is similar to lotus root cross sections. Fig.14 shows examples of surface profiles. The mass loss was about 150mg in each case. In deionized water, a deeply eroded ring area of 1 to 3mm width from the outer circumference is observed. Inside this area, both deep and shallow areas of erosion are mixed. In ethanol, the shape of surface is similar to that in deionized water. In hexane, the surface was clearly divided into deep and shallow areas of erosion.

In conclusion, the mass loss rate can be evaluated in terms of the acoustic impedance if the other conditions are kept constant.

4. CONCLUSIONS

Cavitation erosion tests of silver plated coatings were carried out. The following conclusions are drawn.

(1) The hardness of silver plated coating does not change at temperatures from 303K to 403K. Therefore, the effect of temperature on cavitation erosion is not based on solid material properties, but on properties of the test liquid.
(2) The thermodynamic effect appeared at Σ of 100m/s$^{3/2}$ or more, and the mass loss rate decreased. When Σ decreased below 100m/s$^{3/2}$, the mass loss rate decreased with the decreasing bubble number due to the decrease in the saturated vapor pressure.
(3) The mass loss rate can be evaluated in terms of the acoustic impedance if the other conditions are kept constant.

REFERENCES

1. Kamijo, K., Yamada, H., *Turbomachinery*, Vol.35, No.9 (2007), pp.47-52.
2. Yamada, H., Uchiumi, M., *Turbomachinery*, Vol36, No.2 (2008), pp.3-9.
3. Uchiumi, M., Yamada, H., Kamijo, k., *Turbomachinery*, Vol.38, No.6 (2010), pp.327-333.
4. Kikuchi, M., Hasegawa, T., Nosaka, M., Jinnai, T., *Proceeding of JAST Tribology Conference*, Kanazawa (1994-10), pp.579-582.
5. Hattori, S., Komoriya, I., Kawasaki, S., Kono, S., *Transaction of the JSME*, Series A, Vol.77, No.775 (2011), pp.438-447.
6. Brennen, C., *Transaction of the ASME*, (1973), pp.533-541.
7. Turbomachinery Society of Japan ed., TSJ G 001 (2011), pp.63-64, Turbomachinery Society of Japan.
8. Watanabe, S., Furukawa, A., *Turbomachinery*, Vol.36, No.3 (2006), pp.26-33.
9. Mitutoyo Corporation, Catalog No.17001 http://www.mitutoyo.co.jp/support/service/catalog/index05.html
10. Gross, L.A., *NASA TN D-7451*, (1973).
11. Yoshida, Y., Kikuta, K., Hasegawa, S., Shimagaki, M., and Tokumasu, T., ASTM JFE, Vol.129, (2007), pp.273-278.
12. Yoshida, Y., Nanri, H., Kikuta, K., Kazami, Y., Iga, Y., and Ikohagi, T., *ASTM JFE*, Vol.133, (2011), pp.06130-1-06130-7.
13. Kikuta, K., Yoshida, Y., Hashimoto, T., Nanri, H., Mizuno, T., Shimiya, N., *Transaction of the JSME*, Series B, Vol.76, No.772 (2010), pp.102-110.
14. Franc, J.P., Rebattet, C., and Coulon, A., *ASME JFE*, Vol.126, No.5 (2004), pp.716-723.
15. Hattori, S., Goto, Y., Fukuyama, T., Yagi, Y., Murase, M., *Transaction of JSME*, Series A, Vol.71, No.707 (2005), pp.89-95.
16. Wilson, R.W., and Graham, R., *Conf. Lubrication and Wear*, IME, London (1957), pp.707-712.